RESEARCH

Modelling an unconventional closed-loop deep borehole heat exchanger (DBHE): Sensitivity Analysis on the Newberry Volcanic Setting

Hannah R. Doran[1*], Theo Renaud[2], Gioia Falcone[1], Lehua Pan[3] and Patrick G. Verdin[2]

*Correspondence:
h.doran.1@research.gla.ac.uk
[1]James Watt, School of Engineering, University of Glasgow, G12 8QQ Glasgow, UK
Full list of author information is available at the end of the article

Abstract

Geothermal energy is a baseload resource that has the potential to contribute significantly to the transition to a low-carbon future. Alternative (unconventional) deep geothermal designs are thus needed to provide a secure and efficient energy supply. Current Enhanced Geothermal Systems (EGS) are under technical review as a result of the associated low recovery factors and risk of induced seismicity in connection with reservoir stimulation operations, and Supercritical EGS (SEGS) concepts are still under early research and development. The Newberry and Icelandic Deep Drilling Projects (NDDP and IDDP) aid these developments to drill deeper into very hot temperature zones. An in-depth sensitivity analysis was investigated considering a deep borehole closed-loop heat exchanger (DBHE) to overcome the current limitations of deep EGS. Using the DBHE, cold working fluid is pumped down in the outer annulus and rises to the surface via natural convection or is pumped up via an inner tubing. A T2Well/EOS1 model previously calibrated on an experimental DBHE in Hawaii was adapted to the current NWG 55-29 well at the Newberry volcano site in Central Oregon. A sensitivity analysis was carried out, including parameters such as: the working fluid mass flow rate, the casing and cement thermal properties and the wellbore radii dimensions. The results allow an assessment of key thermodynamics within the wellbore and provide an insight into how heat is lost/gained throughout the system. This analysis was performed under the assumption of sub-critical conditions. Requirements for further software development are briefly discussed, which would facilitate the modelling of unconventional geothermal wells in supercritical systems.

Keywords: Closed-loop deep borehole heat exchanger; EGS; NDDP; T2Well; EOS1

Introduction

Geothermal energy is an ideal candidate to dominate the energy industry in the foreseeable future. Holding a good reputation at providing a constant supply of heat and/or electricity, this mature baseload technology could aid the climate crisis by significantly reducing carbon emissions.

Conventional deep geothermal methods have been utilised to provide power production from natural hydrothermal reservoirs with these desired characteristics: a large heat source, highly permeable, sufficient supply of injected water, impermeable layer of cap rock and a reliable recharge system (DiPippo, 2015). Generally, these sites are unique and restricted by location, severely limiting the true potential

of geothermal energy - according to the International Energy Agency, this resource could generate $1400TWh$ per year by 2050 while avoiding $800Mt$ of CO_2 (IEA, 2011). This largely untapped resource demands alternative solutions to compete in the renewable energy market, specifically exploiting unconventional methods to extract heat, notably from petrothermal sources where permeability and/or porosity are lacking (Falcone et al, 2018). There are significant research gaps for deep unconventional methods where the geothermal gradient is larger than the mean value of $25-30°C/km$ (Olasolo et al, 2016). In an Enhanced Geothermal System (EGS), cold water is injected at high pressure into the subsurface to stimulate fractures, hence creating an artificial reservoir (Olasolo et al, 2016). The first EGS project was in Los Alamos (New Mexico), previously defined as a Hot Dry Rock (HDR) project due to lack of natural water saturation in basement rocks (Breede et al, 2013; Olasolo et al, 2016). EGS's are currently under technical review as they are associated with the risk of inducing seismic activity (Lu, 2018). Examples of abandoned EGS projects due to induced seismicity are the Basel project in Switzerland (Lu, 2018) and the Pohang project in South Korea (Kim et al, 2018). Fundamental research and development on Supercritical EGS (SEGS) is ongoing, such as Iceland's IDDP projects (Reinsch et al, 2017), the Japan Beyond-Brittle Project (Muraoka et al, 2014) and the DESCRAMBLE project in Italy (Bertani et al, 2018). SEGS's involve drilling deeper into regions of partial melt past the brittle-ductile transition zone to achieve a larger flow temperature at the bottom of the wellbore (Cladouhos et al, 2018). Here, the fluid is expected to reach a supercritical state, with no clear distinction between the liquid or vapour phase; for pure water, this corresponds to conditions $T > 374°C$ and $P > 22.1MPa$ (Dobson et al, 2017; Sudarmadi et al, 2012). The development of SEGS's relies on ultra-high temperature technology, capable of withstanding bottomhole temperatures of $430-550°C$, typical of supercritical environments (Lu, 2018). The IDDP-1 well yielded superheated steam at a temperature of $452°C$ and pressure of $140bar$, corresponding to an electricity generation potential of $35MWe$, while in 2017, the IDDP-2 successfully reached supercritical fluids at $426°C$ and $340bar$ at a depth of $4659m$ (DEEPEGS, 2018). However, IDDP-1 drilling was abandoned after hitting a magma intrusion at $900°C$ at $2100m$ and the first flow test of IDDP-2, conducted in December 2019, encountered delays (DEEPEGS, 2018, 2019). Overcoming the challenges posed by these unique resources could potentially unlock a five times greater energy content and a factor of ten times electricity generation potential associated with supercritical fluids at $400°C$ compared with EGS technology at $200°C$ (Cladouhos et al, 2018).

This study focuses on the Newberry Volcano EGS project in Central Oregon. This site was one of the first to consider heat extraction from a volcanic source, in addition to developments in hydroshearing stimulation techniques to mitigate induced seismicity and adapting a thermally-degradable zonal isolation material to isolate fractures from intended stimulated zones (Cladouhos et al, 2016). Figure. 1 shows the two wellbores locations - NWG 55-29 and NWG 46-16 - along the western flank of the volcano.

From Figure 1, the NWG 55-29 was drilled down to $3067m$ with a bottom well temperature of $331°C$ (Cladouhos et al, 2016), at subcritical conditions ($100°C < T < 374°C$ and $0.1MPa < P < 22.1MPa$) (Asl and Khajenoori, 2013), and plans

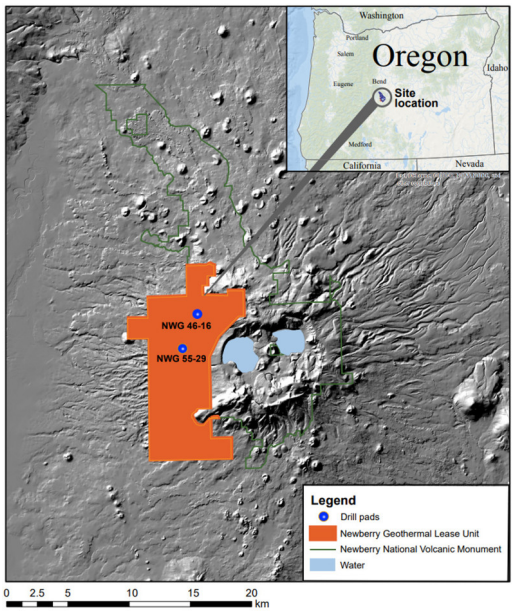

Figure 1 NDDP site NWG 46-16 and NWG 55-29 wellbore locations (Bonneville et al, 2018).

to deepen the NWG 46-16 well to $4877m$ are in place to transition into supercritical environments (Cladouhos et al, 2018). It is important to note that the wells NWG 55-29 and NWG 46-16 are open-loop designs whereby the pumped working fluid is in direct contact with the reservoir.

A low average flow rate of $3.2kg/s$ was obtained from a NWG 55-29 stimulation test, compared to expected conventional EGS flow rates of $50-60kg/s$ (Cladouhos et al, 2016; MIT, 2006). As a result of this and of the potential risk of induced seismicity, a deep closed-loop borehole heat exchanger (DBHE) design was assumed for this study, to be accommodated within the NWG 55-29 open-loop well. The conventional BHE design was conceived for shallow depths and low temperature gradients, for heating and cooling applications (Acuña et al, 2011; Beier et al, 2013; Holmberg et al, 2016). Some DBHE sites already exist, including two deep boreholes in Weissbad and Weggis in Switzerland, at depths of 1.2km and 2.3km respectively (Kohl et al, 2000, 2002). To ensure realistic wellbore properties for the synthetic DBHE in the Newberry settings, casing radii dimensions from these two sites were applied in this study. See the Sensitivity Analysis section for details.

The modelled DBHE involves pumping cold fluid down the outer annulus, such that hot fluid rises to surface up the inner tubing via a thermosiphon effect (natural convection) or through the use of pumps (Tang et al, 2019). The DBHE design was previously modelled in the Villafortuna abandoned oil well in Italy (Alimonti et al, 2016), the KTB deep borehole project setting in Germany (Falcone et al, 2018) and the IDDP-1 well in Iceland (Renaud et al, 2019). Replacing the current NWG 55-29 well with a DBHE would not only mitigate the risks of induced seismicity, but also prevent fluid losses and contamination to the surrounding environment, as the working fluid is not in direct contact with the surrounding rock (Wang et al, 2019). Installation costs can also be reduced by decreasing the boreholes

thermal resistance via a thermally enhanced outer pipe in ground-coupled heat pump systems (Raymond et al, 2015). A heat conducting filler of graphite could also be implemented around the DBHE design to enhance downhole heat transfer (Falcone et al, 2018).

Former DBHE studies have relied upon numerical or analytical methods to discretise the geothermal system into elements within a grid (Alimonti et al, 2018). A research code T2Well/EOS1, recently developed at Lawrence Berkeley National Laboratory for simulating coupled wellbore-reservoir processes involved in geothermal systems, was adopted in this study to model appropriate subcritical conditions in the Newberry volcano area.

Methods

The DBHE was modelled into the Newberry geothermal system with a 2D axisymmetric MESH adopting T2Well/EOS1 (Pan and Oldenburg, 2014). The model set-up is described below.

Mathematical Model

T2Well/EOS1 is an integrated wellbore-reservoir numerical simulator to simulate non-isothermal flows of multi-phase fluids (steam-water) in both domains simultaneously (Pruess et al, 2012). T2Well was previously used to model various contexts, such as heat extraction in a closed-loop system with supercritical CO_2 as the working fluid (Higgins et al, 2016) and for a gas storage blow out (Pan et al, 2018). The equation of state (EOS1) was utilised, representing one non-isothermal water component under two-phase conditions (Pruess et al, 2012). The applied thermodynamic equations within the reservoir are similar to those used in other TOUGH2 family code and are defined in Table 1.

Table 1 Key reservoir equations

$$\frac{d}{dt}\int_{V_n} M^\kappa dV_n = \int_{\Gamma_n} F^\kappa \cdot n d\Gamma_n + \int_{V_n} q^\kappa dV_n \tag{1}$$

$$M^m = \phi(S_L\rho_L X_L^\kappa + S_G\rho_G X_G^\kappa \tag{2}$$

$$F^m = X_L^\kappa \rho_L u_L + X_G^\kappa \rho_G u_G \tag{3}$$

$$M^E = (1-\phi)\rho_R c_R T + \phi(\rho_L S_L U_L + \rho_G S_G U_G) \tag{4}$$

$$F^E = -\lambda\nabla T + h_L\rho_L u_L + h_G\rho_G u_G \tag{5}$$

$$u_{ph} = -\frac{k_a k_{r,ph}}{\mu_{ph}}(\nabla P_{ph} - \rho_{ph} g) \tag{6}$$

Equation (1) depicts the general mass and energy conservation equation with M^m, F^m, M^E and F^E in Equations (2) to (5) representing the mass accumulation, mass flux, energy accumulation and energy flux terms respectively (Renaud et al, 2020). The phase velocity u_{ph} in Equation (6) is solved by adopting a 3D multi-phase Darcy flow for a heterogeneous porous media.

The key equations for the wellbore used in T2Well/EOS1 are defined in Table 2. Equation (7) depicts the conservation equation in partial derivative form, with M^E defined in Equation (8) and F^E in Equation (9) representing the energy accumulation and flux terms, respectively (Renaud et al, 2020).

Table 2 Key wellbore equations

$$\frac{\partial M^\kappa}{\partial t} = q^\kappa + F^\kappa \tag{7}$$

$$M^E = \rho_L S_L (U_L + \frac{u_L^2}{2} + gz\cos\theta) + \rho_G S_G (U_G + \frac{u_G^2}{2} + gz\cos\theta) \tag{8}$$

$$F^E = -\lambda \frac{\partial T}{\partial z} - \frac{1}{A}\frac{\partial}{\partial z}[A\rho_L S_L u_L (h_L + \frac{u_L^2}{2} + gz\cos\theta) + A\rho_G S_G u_G (h_G + \frac{u_G^2}{2} + gz\cos\theta)] \tag{9}$$

The Drift-Flux model (DFM) is used in solving the two-phase momentum conservation equation in the wellbore. A relationship is assumed between the gas velocity (u_G) and the volumetric flux of the mixture (j):

$$u_G = C_0 j + u_d \tag{10}$$

The liquid velocity u_L can then be calculated from j and the drift velocity u_d as:

$$u_L = \frac{1 - S_G C_0}{1 - S_G} j - \frac{S_G}{1 - S_G} u_d \tag{11}$$

The drift velocity is thus calculated as (Pan et al, 2005):

$$u_d = \frac{(1 - C_0 S_G) u_c K(S_G, K_u, C_0) m(\theta)}{C_0 S_G \sqrt{\rho_G / \rho_L} + 1 - C_0 S_G} \tag{12}$$

The velocities u_G and u_L within the mixture are then solved with u_d to obtain the momentum conservation equation; simplified to Equation (13)(Akbar et al, 2016; Pan et al, 2011):

$$\frac{\partial}{\partial t}(\rho_m u_m) + \frac{1}{A}\frac{\partial}{\partial z}[A(\rho_m u_m^2 + \gamma)] = -\frac{\partial P}{\partial z} - \frac{\Gamma f \rho_m |u_m| u_m}{2A} - \rho_m g \cos\theta \tag{13}$$

Table 3 defines the remaining parameters from the drift flux model, extracted from (Pan and Oldenburg, 2014). The mass and energy conservation equations are solved using the Newton Raphson iteration process (Pruess et al, 2012).

Table 3 Key drift flux parameters in Equation (13)

Description	Equation
Slip between two phases	$\gamma = S_G(\rho_G\rho_L\rho_m/\rho_m^{*2})[(C_0-1)u_m + u_d]^2/(1-S_G)$
Mixture density	$\rho_m = S_G\rho_G + (1-S_G)\rho_L$
Mixture velocity	$u_m = [S_G\rho_G u_G + (1-S_G)\rho_L u_L]/\rho_m$
Adjusted average density of mixture	$\rho_m^* = S_G C_0\rho_G + (1-S_G C_0)\rho_L$

Newberry case-study

The DBHE was modelled into the Newberry geothermal system by replacing the NWG 55-29 well with the unconventional closed-loop design. The DBHE model built with T2Well/EOS1 is based on an experimental study from (Morita et al, 1992b), whereby the measured and computed pressure and temperature values were verified with the HGP-A well site in Hawaii (Morita et al, 1992b). The DBHE design is presented in Figure 2, alongside the 2D axisymmetric grid representation; note Casg1 is the inner casing separating the outer annulus and the inner tubing and Casg2 is the external casing separating the outer annulus and the cement (Ceme1).

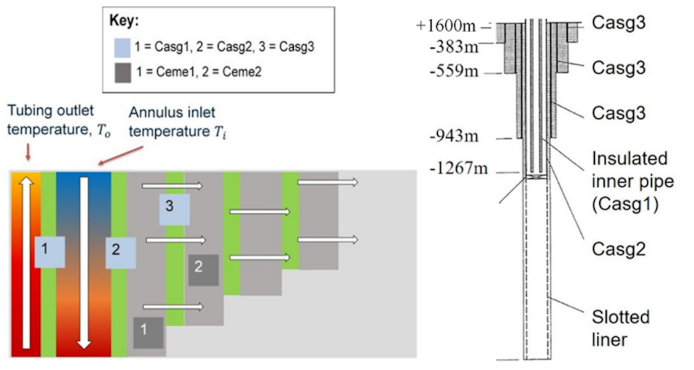

Figure 2 DBHE design implemented in T2Well/EOS1. Left - 2D asymmetric MESH containing 2752 cells in the r $(1-200m)$ and z $(+1599.50m\ to-1580m)$ axis, interpreted from (Morita et al, 1992b; Sonnenthal et al, 2012). **Right** - Well completion diagram of the DBHE interpreted from (Cladouhos et al, 2016). Both depict the casing and cement sections at appropriate elevations in T2Well/EOS1, interpreted from (Tang et al, 2019; Toth, 2015).

The DBHE model was based on the Newberry 55-29 well from (Cladouhos et al, 2016). The original completion diagram from (Morita et al, 1992b) was altered to account for the increase in depth from $879.5m$ to the NWG 55-29 wellbore depth of $3067m$ (Cladouhos et al, 2016). Figure 2 highlights key elevation depths for each section to account for these changes. The slotted liner was removed in the model and the bottom of the well reached an elevation of $-1267m$.

The Newberry geothermal area was defined according to the thermal-hydrological-chemical model adopted from (Sonnenthal et al, 2012). Four geological zones were highlighted within the volcanic area and incorporated into the model at the specified elevation with known thermodynamic properties obtained from (Sammel et al,

1988; Sonnenthal et al, 2012). Properties such as porosity ϕ, permeability k, specific heat capacity c_P and thermal conductivity λ were tabulated in (Doran, 2019; Renaud et al, 2020). Thermodynamic wellbore properties were also incorporated from (Morita et al, 1992a) where ϕ, k, c_P, λ and density ρ were tabulated in (Doran, 2019). Water was injected into the outer annulus at a temperature of $12°C$ with an imposed mass flow rate $\dot{m}$.

The top boundary condition of the reservoir model was set with a surface temperature of $12°C$ and a surface atmospheric pressure of $1bar$ (Sonnenthal et al, 2012). The default pressure for the boundary condition on the DBHE was set to $3bar$ to prevent effects from local vacuum conditions reaching the lower limit of the code. Only heat flow was considered between the wellbore and reservoir to reflect the closed-loop design, excluding fluid flow. As shown in (Sonnenthal et al, 2012), the upper part of the reservoir was defined by constant thermodynamic values. It was assumed in the model that the pressure and temperature were constant at elevation $+1600m$, neglecting the pressure and thermal losses in the water table defined between $+1800m$ and $+1600m$.

T2Well numerical validation

Experimental validation

The experimental data from a DBHE in Hawaii set at the depth of $879.6m$ was used to validate the T2Well model (Morita et al, 1992b). The pressure and temperature distribution in the first 12 hours showed a good match between measured values and simulations as illustrated in Figure 3. Model properties and details can be found in (Renaud et al, 2020).

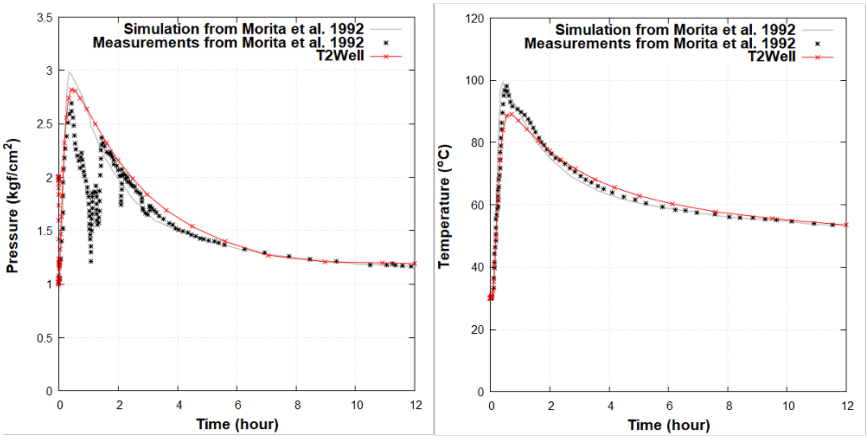

Figure 3 Left - Transient pressure simulation with T2Well compared to measurements from (Morita et al, 1992b).**Right** - Transient temperature simulation with T2Well compared to measurements from (Morita et al, 1992b)

Numerical discussion

A DBHE with graphite on the wellbore was numerically investigated using FEFLOW (Falcone et al, 2018). While authors in (Falcone et al, 2018) used constant water properties, T2Well uses the pressure and temperature dependent thermophysical properties based on models suggested by the International Formulation

Committee (IFC, 1967). As stated in (Sui et al, 2019; Tang et al, 2019), constant fluid properties seem to generate errors in the pressure losses calculation and heat produced in DBHEs. The produced water temperature and heat flux were underestimated for a DBHE of $6100m$ (Alimonti and Soldo, 2016) and overestimated by 11% in a DBHE of $3500m$ (Hu et al, 2020). These errors occurred due to not accounting for specific heat capacity and density changes within the DBHE. Compared with constant water properties, these changes would increase the total heat energy while decreasing the temperature of the return fluid.

The same deep geothermal system was modeled based on the KTB deep borehole project, reaching a reservoir depth of $8000m$ (Falcone et al, 2018), using T2Well/EOS1. While a 3D model was considered in (Falcone et al, 2018), the T2Well model used in this work is an axisymmetric RZ mesh centred on the wellbore. Graphite is implemented with a thermal conductivity value of $300W/m.K$ and an assumed porosity of 1%.

The T2Well grid contains 1030 elements. The maximum radial extension of the model is 1 km. The bottom of the DBHE was set at a depth of $7000m$. Water was injected in the annulus at the flow rate of $304.8m^3/d$ ($\sim 7kg/s$). The reservoir was assumed to be fully saturated water. The surface temperature was set to 15°C, with an initial temperature gradient of $40°C$/km. The bottom temperature is $330°C$. The graphite filled the surrounding of the DBHE from the depth of 4400 and $7200m$ instead of the cement or grout. The value of casing materials is $900J/kg.K$ and the wall roughness is $2.5 \times 10^{-5}m$. The thermal properties of the rock and DBHE sections applied in the model can be found in (Falcone et al, 2018; Seyidov, 2016). Fig. 4 describes the water temperature at the surface of the DBHE compared to the FEFLOW results.

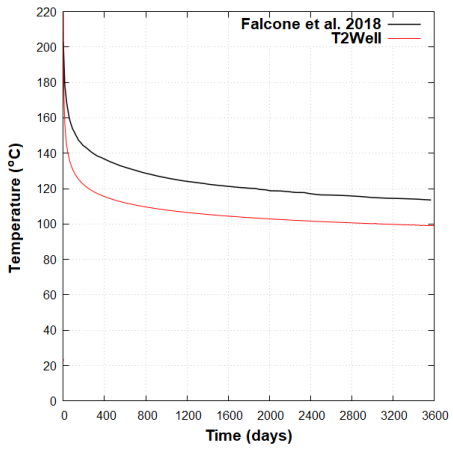

Figure 4 Numerical results comparison from (Falcone et al, 2018) and the T2well/EOS1 model.

From this case study, the temperature obtained at the surface of the DBHE was lower than previously described in (Falcone et al, 2018), suggesting the potential overestimation of the water temperature using constant water properties due to changes in the specific heat value (Song et al, 2018). As stated by (Hu et al, 2020), the temperature dependent properties as calculated in T2Well/EOS1, must be considered for long term performance evaluation of DBHE.

Sensitivity Analysis

Table 4 summarises the parameters investigated in this study: mass flow rate of water $\dot{m}(kg/s)$, thermal conductivity $\lambda(W/mK)$ of the casings and cement (see Figure 2), and the wellbore inner $r_i(m)$ and outer $r_o(m)$ radii dimensions for the annulus and tubing. All parameter changes were referenced against a base case scenario from (Morita et al, 1992b).

The working fluid velocity u_F at the bottom of the well was explored for values $3kg/s < \dot{m} < 9kg/s$ (See Mass Flow rate section).

An insulated inner casing is advantageous for preventing heat losses between the inner tubing and the outer annulus, hence maximising the extracted energy flow rate at the outlet (Falcone et al, 2018; Song et al, 2018). Therefore, the effectiveness of an insulated inner casing as inner tubing for the DBHE was investigated by adjusting $\lambda(W/m.K)$ of Casg1 whilst $\dot{m}$ was fixed at $5kg/s$. Note $46.1W/m.K$ was chosen as an upper limit to explore the heat transfer through the design when all three casing properties are identical - Casg2 = Casg3 at $\lambda = 46.1W/m.K$ - (see Inner casing properties section).

Fixing Casg1 at $\lambda = 0.01038W/m.K$ and $\dot{m} = 5kg/s$, the outer casing thermal conductivity λ was adjusted based on quoted values in Table 4. The casing properties extracted from the Weissbad DBHE and the NWG 55-29 well were explored here (see Outer casing properties section).

Fixing $\dot{m}$, Casg1 and Casg2 properties to the base case values quoted in Table 4, the thermal conductivity λ parameter for various cements was explored. The use of a heat conducting filler for enhanced heat transfer (graphite flakes positioned laterally and parallel to one another) was also investigated (Falcone et al, 2018) at $\lambda = 300W/m.K$ (see Cement properties section).

Four wellbore radii cases were investigated: annulus reduction (Case 1), annulus increase (Case 2), tubing increase (Case 3) and tubing reduction (Case 4) against the base case radii dimensions from (Morita et al, 1992b). Again, the mass flow rate was fixed at $\dot{m} = 5kg/s$. Case 1 involved an annulus reduction by 1.27, incorporating $r_i = 0.0629m$ from the Weggis plant (Kohl et al, 2002). Case 2 involved an annulus increase by 1.33 by implementing $r_i = 0.1061m$ from the Weissbad well (Kohl et al, 2000). Case 3 values were chosen so the tubing increase factor was equal to that of Case 2 (1.33). Case 4 tubing reduction by 1.22 was influenced by $r_o = 0.0365m$ tubing dimensions from the Weggis well (Kohl et al, 2002). For all radii changes, the annular space between r_i and r_o remained constant at $0.0092m$ and $0.0192m$ for the annulus and tubing respectively.

The heat transfer down the outer annulus and up the inner tubing was investigated for each parameter change and compared to the base case scenario from (Morita et al, 1992b) seen in Table 4. For each parameter change, the temperature $T(°C)$ and pressure P(MPa) vs elevation (m) was investigated over a total simulation time of 30 years. In addition, the simulated energy flow rate of the wellbore $q_{Th}(MW)$ was also extracted from the output file. A review on the energy flow rate for the closed-loop DBHE vs open-loop NWG 55-29 wellbore was explored and concludes this

Table 4 Parameter changes investigated in the DBHE model.

Parameters	Values	Description	Base case
$\dot{m}(kg/s)$	3-5-7-9		5
Inner casing properties			
Casg1 $\lambda(W/mK)$	0.01038	Insulated [1]	0.01038
	1.163	Morita [2]	
	2.5		
	46.1	Morita [3]	
Outer casing properties			
Casg2-3 $\lambda(W/mK)$	46.1	Morita [2]	46.1
	45.0	Weissbad [4]	
	15.0	Newberry [5]	
	0.01038	Insulated [1]	
Cement properties			
Ceme 1-2 $\lambda(W/mK)$	0.99	Morita [3]	0.99
	2.24	REF concrete [6]	
	3.52	GRAP concrete [6]	
	300	Graphite flakes [1]	
Radii			
Annulus radii $r_i/r_o(m)$	0.0797/0.0889	Morita	0.0797/0.0889
	0.0629/0.0721	Case 1	
	0.1061/0.1153	Case 2	
	0.0797/0.0889	Case 3	
	0.0797/0.0889	Case 4	
Tubing radii $r_i/r_o(m)$	0.0253/0.0445	Morita	0.0253/0.0445
	0.0253/0.0445	Case 1	
	0.0253/0.0445	Case 2	
	0.0336/0.0528	Case 3	
	0.0173/0.0365	Case 4	

[1] Insulated inner casing $0.01038W/mK$, cited from (Falcone et al, 2018).
[2] Thermal conductivity values quoted from (Morita et al, 1985).
[3] Thermal conductivity values quoted from (Morita et al, 1992a).
[4] Weissbad parameters quoted from (Kohl et al, 2000).
[5] Newberry parameters quoted from (Cladouhos, 2012).
[6] Cement parameters obtained from (Asadi et al, 2018).

study. The energy flow rate is estimated for the NWG 55-29 wellbore by adopting equation (14) below:

$$q_{Th} = c_P \dot{m} \Delta T \tag{14}$$

Where $\Delta T = T_o - T_i$, $T_o = 94°C$ representing the first flow back temperature recorded at the outlet point of the NWG 55-29 wellbore (Cladouhos et al, 2016) and $T_i = 12°C$ is the surface temperature of the Newberry environment (Sonnenthal et al, 2012). $c_P = 4200 J/kg°C$ is assumed a constant for pure water properties. See Energy flow rate comparison between DBHE and NWG 55-29 section for details.

Results

Mass flow rate

Figure 5 shows the temperature and pressure distributions along the DBHE for varied $\dot{m}$. Table 5 highlights key thermodynamic properties from Figure 5 and the simulation output file: ΔT between inlet T_i and outlet T_o points, energy flow rate q_{Th} and the working fluid velocity u_F at the bottom of the wellbore:

From Figure 5, it appears that an increase in $\dot{m}$ results in a lower bottom well temperature ($32°C$ for $9kg/s$ in comparison to $73°C$ for $3kg/s$). This decrease is

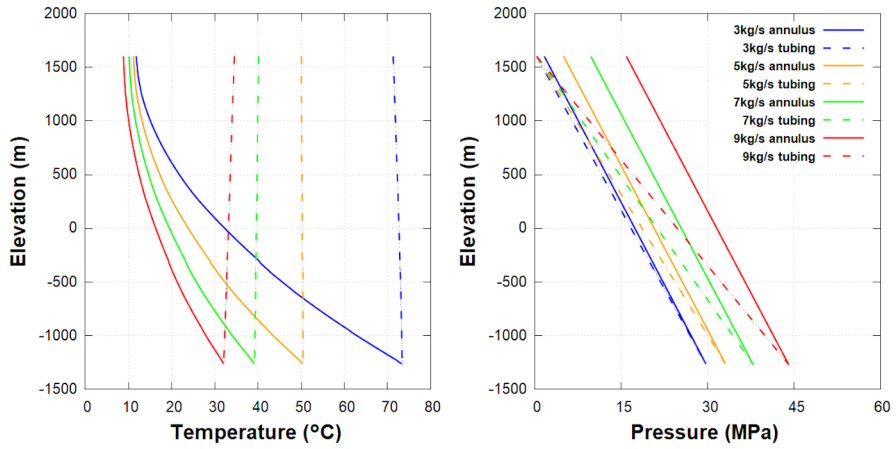

Figure 5 Mass flow rate analysis over 30 years. Left - Temperature vs Elevation for various $\dot{m}(kg/s)$. **Right** - Pressure vs Elevation for various $\dot{m}(kg/s)$. Solid lines represent annulus and dashed lines tubing data respectively. Legend applies to both graphs. All cases were compared with the base-case graph (in yellow).

Table 5 Key thermodynamic properties for various $\dot{m}(kg/s)$ quoted to 3 significant figures (3.s.f)

$\dot{m}(kg/s)$	$\Delta T(^{\circ}C)$	$q_{Th}(MW)$	$u_F(m/s)$
3	59.6	1.14	1.51
5	38.9	1.46	2.48
7	30.0	1.76	3.45
9	25.7	2.06	4.42

observed in response to an increase in working fluid velocity ($4.42m/s$ vs $1.51m/s$), leading to a shorter residence time. An increased $\dot{m}$ up the tubing results in a lower outlet temperature ($34.5^{\circ}C$ for $9kg/s$ in comparison to $71.4^{\circ}C$ for $3kg/s$). A slight gain in temperature up the tubing is also observed (a $2.48^{\circ}C$ increase for $9kg/s$ in comparison to a $2.06^{\circ}C$ decrease for $3kg/s$). This could be due to a higher pressure reduction up the tubing ($\Delta P = 43.7MPa$ for $9kg/s$ vs $\Delta P = 29.4MPa$ for $3kg/s$).

A mass flow rate value of $9kg/s$ displays the highest q_{Th} compared with $3kg/s$ and yields the largest ΔT up the tubing. Ideally, ΔT should be minimised up the tubing to enhance the systems efficiency by extracting more heat from the surrounding formations. A balance between efficiency and energy flow rate should be achieved. Due to $9kg/s$ causing too high of a friction loss up the tubing and inducing higher pumping costs as shown by an increased inlet pressure ($15.9MPa$ as opposed to $1.62MPa$ for $3kg/s$), and $3kg/s$ yielding the lowest energy flow rate ($1.14MW$), $5kg/s$ is considered the best-case scenario with minimal ΔT up the tubing and an energy flow rate of $q_{Th} = 1.46MW$.

Inner casing properties

Figure 6 shows the temperature and pressure distributions along the DBHE for varied λ in Casg1. Table 6 summarises key thermodynamic properties extracted from Figure 6 and from the simulation output file: ΔT between inlet (T_i) and outlet (T_o) points and the energy flow rate q_{Th}.

ΔT down the annulus is seen to increase while λ increases in Casg1 ($\Delta T = 39.2^{\circ}C$ for $\lambda = 0.01038W/m.K$ compared with $\Delta T = 216^{\circ}C$ for $\lambda = 46.1W/m.K$). This

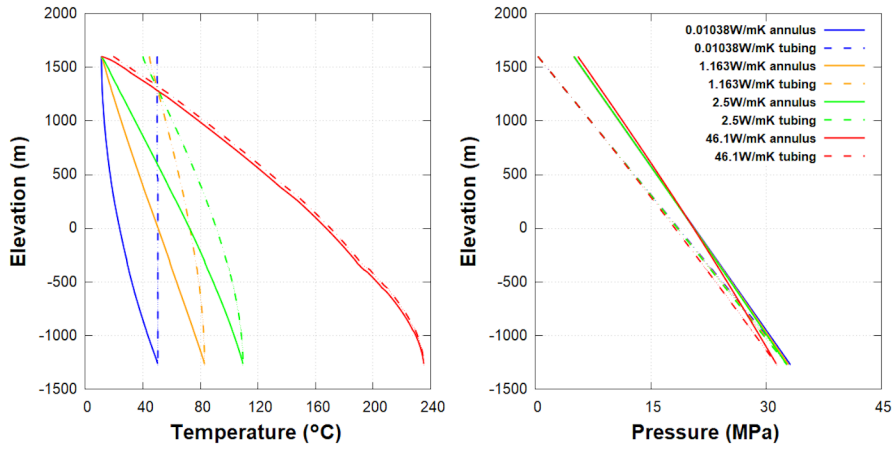

Figure 6 Thermal conductivity analysis in inner casing (Casing 1) over 30 years Left - Temperature vs Elevation for various $\lambda(W/mK)$. **Right** - Pressure vs Elevation for various $\lambda(W/mK)$. Solid lines represent annulus and dashed lines tubing data respectively. Legend applies to both graphs. All cases were compared to the base-case graph (in blue).

Table 6 Key thermodynamic properties for various $\lambda(W/mK)$ quoted to 3.s.f

$\lambda(W/mK)$	$\Delta T(°C)$	$q_{Th}(MW)$
0.01038	38.9	1.46
1.163	33.3	1.35
2.5	28.8	1.25
46.1	8.19	0.830

is in agreement with Fourier's law of heat conduction (Nuclear-power.net, 2019) via an increase in heat transfer from the reservoir into the wellbore. The inlet pressure remains approximately constant at $5MPa$ due to the constant mass flow rate of $5kg/s$ imposed. In addition, the outlet pressure remains constant at $0.3MPa$. Using a thermal conductivity $\lambda > 0.01038W/m.K$, the temperature up the tubing significantly reduces as a result of low thermal insulation between the annulus and tubing (Song et al, 2018). For maximum efficiency, ΔT should be minimised to follow an isothermal process to surface. In fact, $\lambda = 46.1W/mK$ is considered the worst-case scenario when all casing properties are identical and thermal insulation is at its lowest. A higher λ yields a smaller ΔT between the inlet and outlet points and hence a smaller energy flow rate q_{Th} ($0.830MW$ vs $1.46MW$), again due to poor thermal insulation. Therefore, minimising the thermal conductivity in Casg1 ($\lambda = 0.01038W/mK$) is the best-case scenario to achieve maximal bottomhole T and preventing significant cooling of the fluid up the tubing.

Outer casing properties

Figure 7 displays the temperature and pressure distributions along the DBHE for varied λ in the outer casing. The first three parameter changes result in nearly identical temperature and pressure profiles. Therefore, two cases were compared: $\lambda = 0.01038W/m.K$ for the inner Casg1 only (red), and for all casings (green). Table 7 highlights key thermodynamic properties from Figure 6 and the output file: ΔT between inlet T_i and outlet T_o points, the inlet P_i and outlet P_o pressure points and the simulated energy flow rate q_{Th} for these two cases.

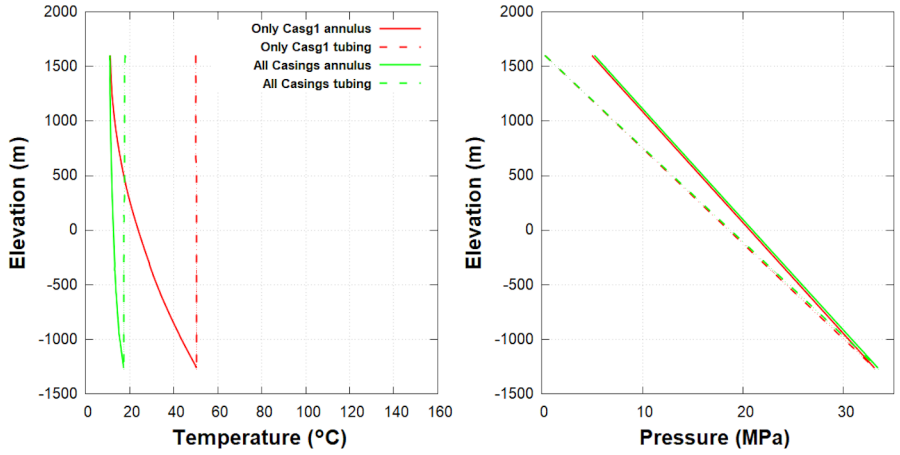

Figure 7 Thermal conductivity analysis in outer casings for fixed $\dot{m} = 5(kg/s)$ over 30 years. **Left** - Temperature vs Elevation for various $\lambda(W/mK)$. **Right** - Pressure vs Elevation for various $\lambda(W/mK)$. Solid lines represent annulus and dashed lines tubing data respectively. The base-case graph here is highlighted in red.

Table 7 Key results comparing insulating properties for only Casg1 and for all casings to 3.s.f

Key Results	Only Casg1	All Casings
$T_i(°C)$	11.1	10.9
$T_o(°C)$	50.0	17.8
$\Delta T(°C)$	38.9	6.92
$P_i(MPa)$	4.97	5.23
$P_o(MPa)$	0.302	0.302
$q_{Th}(MW)$	1.46	0.785

When all casings are insulated at $\lambda = 0.01038W/m.K$, a lower bottomhole temperature ($17.2°C$ vs $50.4°C$) is observed in addition to a lower outlet temperature ($T_o = 17.8°C$ vs $T_o = 50.0°C$). This is due to insufficient heat transfer between the reservoir and wellbore. ΔT between the inlet and outlet points decreases approximately by a factor of 6 ($6.92°C$ vs $38.9°C$) and hence results in a reduction in q_{Th} ($0.785MW$ vs $1.46MW$) as the water fails to gain significant temperature down the annulus when all casings are insulated. Therefore, to ensure an efficient thermal recovery, the best-case scenario is observed when only the inner casing is insulated at $\lambda = 0.1038W/mK$ compared to all casing. This is because Casg1 is most sensitive to ΔT up the tubing - as seen in Mass flow rate section above.

Cement properties

Figure 8 shows the temperature and pressure distributions along the DBHE for varied λ cement properties (Ceme1 and Ceme2 in Figure 2). Key thermodynamic properties extracted from Figure 8 and from the simulation output file are summarised in Table 8: ΔT between inlet T_i and outlet T_o points, and the simulated energy flow rate q_{Th}.

The bottomhole temperature down the annulus increases from $50.4°C$ to $60.9°C$ for $\lambda = 0.99W/m.K$ and $\lambda = 300W/m.K$ respectively. Hence, T_o increases as a result of an increase in λ within the cement, suggesting this parameter change enhances the amount of heat transfer between the reservoir and working fluid. In

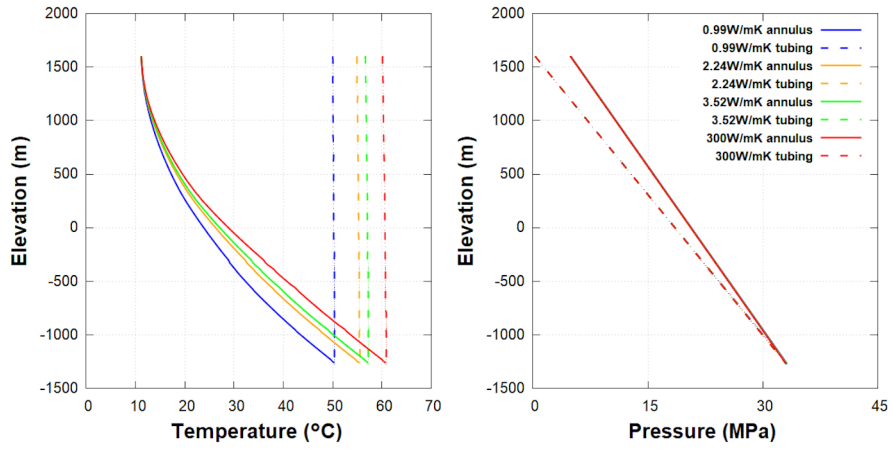

Figure 8 Thermal conductivity analysis in cement layers for fixed $\dot{m} = 5(kg/s)$ over 30 years. **Left** - Temperature vs Elevation for various $\lambda(W/m.K)$. **Right** - Pressure vs Elevation for various $\lambda(W/m.K)$. Solid lines represent annulus and dashed lines tubing data respectively. Legend applies to both graphs. The base-case graph here is highlighted in blue.

Table 8 Key thermodynamic properties for various $\lambda(W/m.K)$ to 3.s.f

$\lambda(W/m.K)$	$\Delta T(°C)$	$q_{Th}(MW)$
0.99	38.9	1.46
2.24	43.8	1.57
3.52	45.5	1.60
300	49.0	1.67

particular, this heat transfer is hindered when λ is lower than that of the reservoir, as identified in Song et al. 2018 (Song et al, 2018). As λ predominantly affects T and not P (as seen in Inner tubing properties section), the pressure distribution along the DBHE shows similar results for all parameter changes. Referring to Table 8, λ is maximised in conjunction with q_{Th}, with a percentage increase of 14.4% comparing conventional cement with a graphite heat conductive filler ($1.67MW$ for $\lambda = 0.99W/m.K$ vs $1.46MW$ for $\lambda = 300W/m.K$). While the use of graphite significantly empowers the heat transfer in the DBHE design, its use as a cement additive is an unproved concept. Therefore, $\lambda < 3.52W/m.K$ parameters are deemed more reasonable as best-case scenario's because conventional cement falls into the region of $0.2 < \lambda < 3.63W/m.K$ (Ichim et al, 2016).

Radii

Figure 9 shows the temperature and pressure distributions along the DBHE for varied radii. Two key scenarios were analysed: varying annulus radii (Case1 and Case2) and increasing annulus and tubing radii by a constant factor of 1.33 (Case2 and Case3). Each scenario was then compared to the original base-case radii from (Morita et al, 1992b), with a constant mass flow rate $\dot{m} = 5kg/s$. Table 9 and Table 10 highlight the key thermodynamic properties from Figure 9 and the output file for each scenario respectively: ΔT between inlet T_i and outlet T_o points, the inlet P_i and outlet P_o pressure points, the simulated energy flow rate q_{Th} and the working fluid velocity u_F at the bottom of the well.

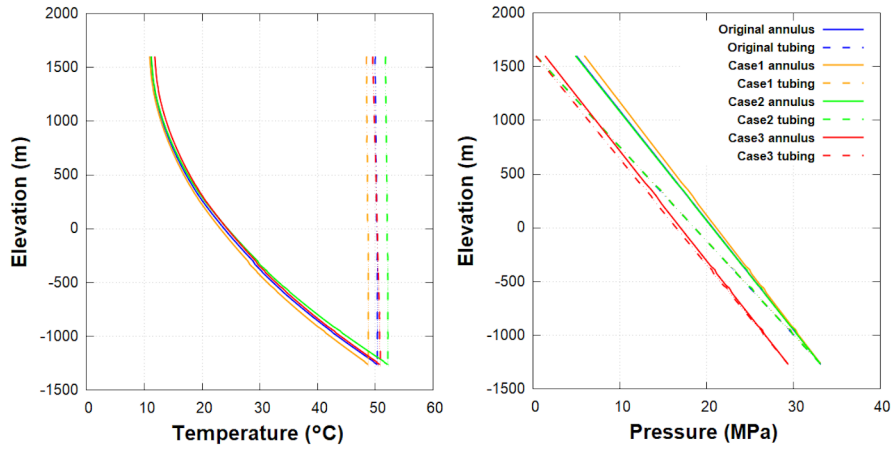

Figure 9 Radii analysis for fixed $\dot{m} = 5(kg/s)$ over 30 years. Left - Temperature vs Elevation for the original, annulus reduction (Case1), annulus increase (Case2) and tubing increase (Case3) radii. **Right** - Pressure vs Elevation for the same cases. Solid lines represent annulus and dashed lines for tubing data respectively. Legend applies to both graphs. The Original case (in blue) represents the base-case scenario.

Table 9 Key results when varying annulus with original radii dimensions to 3.s.f

Key Results	Original	Case1	Case2
$T_i(°C)$	11.1	10.9	11.2
$T_o(°C)$	50.0	48.5	51.8
$\Delta T(°C)$	38.9	37.6	40.6
$P_i(MPa)$	4.97	5.90	4.87
$P_o(MPa)$	0.302	0.302	0.302
$u_F(m/s)$	2.48	2.48	2.48
$q_{Th}(MW)$	1.46	1.43	1.50

Table 10 Key results when increasing annulus and tubing by 1.33 with original radii dimensions to 3.s.f

Key Results	Original	Case2	Case3
$T_i(°C)$	11.1	11.2	11.8
$T_o(°C)$	50.0	51.8	49.6
$\Delta T(°C)$	38.9	40.6	37.8
$P_i(MPa)$	4.97	4.87	1.35
$P_o(MPa)$	0.3025	0.302	0.300
$u_F(m/s)$	2.48	2.48	1.41
$q_{Th}(MW)$	1.46	1.50	1.45

Concerning the annulus comparison in Table 9, the bottomhole temperature decreases from $50.4°C$ to $48.8°C$ alongside a radii reduction (Case1) and increases to $52.3°C$ alongside a radii increase (Case2). This occurs due to variation in the annulus area. For Case2, the annulus area increase consequently increases the working fluid contact surface area. This leads to a longer residence time and hence enhanced heat transfer within the wellbore, as discussed in (Nalla et al, 2005). T_o also shows this trend, decreasing from $50.0°C$ to $48.5°C$ for Case1 and increasing to $51.8°C$ for Case2. Despite the bottom working fluid velocity being constant at $2.48m/s$, the velocity down the annulus will differ due to the radii change. Observing the velocity before it reaches the bottom, it is clear that an increase is observed ($0.363m/s$ vs $0.803m/s$) for an annulus reduction (Case1) and a decrease ($0.363m/s$ vs $0.171m/s$) for an annulus increase (Case2), see Figure 10.

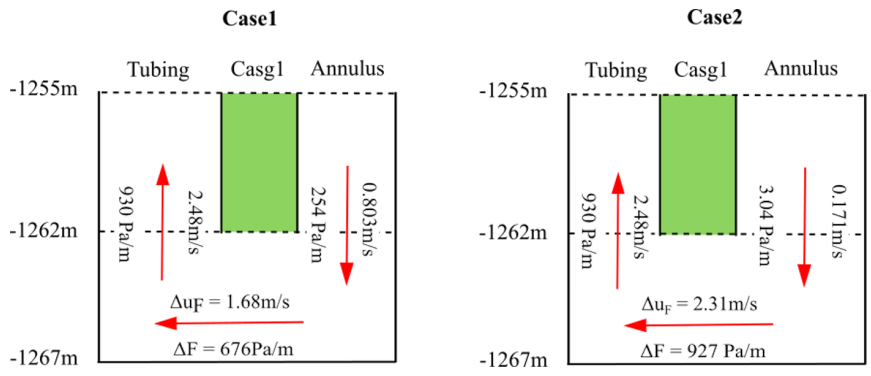

Figure 10 Illustration for Cases 1 and 2 at the bottom of the well. Working fluid velocity u_F and frictional pressure F values are shown for Cases 1 and 2. These values were extracted from the output files for connections between the bottom cell and the one above, as depicted by the red vertical arrows. The horizontal arrow is not modelled in T2Well/EOS1 but is here to represent the differences between the two cells. This image is not to scale.

P_i is seen to slightly increase from $4.97MPa$ to $5.90MPa$ for a radii reduction (Case1) and decrease from $4.97MPa$ to $4.87MPa$ for a radii increase (Case2) due to changes in contact surface area. However, both Case1 and Case2 reach an equal bottomhole pressure of $33.1MPa$ which results in $P_o \approx 0.302MPa$ for both cases.

q_{Th} increased from $1.46MW$ to 1.50 alongside a radii reduction (Case1) and slightly decreased to $1.45MW$ for a radii increase (Case2). The former is influenced by the working fluid's gain in velocity from a decrease in contact surface area by a factor of 1.72, in addition to a larger δT between inlet and outlet points. Therefore, a radii reduction in the annulus (Case2) is the best-case scenario here for maximal energy flow rate.

Case4 (tubing reduction by 1.22) failed to run for $\dot{m} = 5kg/s$ due to a change in pressure into the wellbore that exceeded the limits of the software, $1000bars$ (Renaud et al, 2018). For a constant $\dot{m} = 5kg/s$, at time $t = 0$, the pressure seen at the bottom of the well was $0.25 \times 10^8 Pa$ but below the DBHE in the surrounding formation the pressure reached $1 \times 10^9 Pa$, i.e. $1000bars$. Therefore, Table 10 summarizes the results when the annulus and tubing were increased by an equal factor of 1.33 (Case2 and Case3 respectively).

Temperature down the annulus is seen to slightly increase from $50.4°C$ to $52.3°C$ for the annulus increase (Case2) and a slight increase to $50.9°C$ for a tubing increase (Case3). Again, this is due to adjusting the annulus area as explained above. For instance, Case3 exhibits a smaller annulus radius compared with Case2, leading to a lower bottomhole temperature from a reduction in the working fluid's velocity ($1.41m/s$ vs $2.48m/s$). T_o is also seen to increase from $50.0°C$ to $51.8°C$ for Case2 and decrease to $49.6°C$ for Case3.

Case3 exhibits a smaller P_i compared with Case2 ($1.35MPa$ vs $4.87MPa$). This is again due to Case3 acquiring a smaller annulus radius, reducing the contact surface area and the working fluid's velocity at the inlet point - and hence a lower inlet pressure compared with Case2.

q_{Th} is seen to be nearly identical at $1.46MW$ for Case3 and the original radii. However, Case2 is observed to have a slight increase at $q_{Th} = 1.50MW$ due to

a higher ΔT between inlet and outlet points. It can be inferred that when the tubing radii increases, there is little influence on the value of q_{Th} apart from a slight heat loss up the tubing. On the contrary, the annulus radii increase heavily influences the extent of heat transfer down the annulus and offers a higher q_{Th} from an increased bottomhole temperature. The best-case scenario concluded here is for a radii increase in the annulus (Case2). However, despite an increase in energy efficiency, high drilling costs can incur when adjusting the radii according to (Nalla et al, 2005).

It is worth noting that the assumption of a constant wellbore radius along the wellbore is only a preliminary step, as wells are conventionally drilled with decreasing diameter sections at increasing depths (Nalla et al, 2005). However, keeping a constant radius for the entirety of the wellbore depth simplifies the model, as experimented in (Morita et al, 1992b).

Energy flow rate comparison between DBHE and NWG 55-29

Assuming an average flow rate of $3.2kg/s$, and $\Delta T = 94 - 12 = 82°C$ obtained from the first NWG 55-29 flow back test (Cladouhos et al, 2016), in addition to $c_P = 4200J/kg°C$ for pure water, the energy flow rate obtained at the wellhead of NWG 55-29 is approximately $q_{Th} = 1.10MW$. Comparing this to the DBHE results at $3kg/s$ - $q_{Th} = 1.14MW$ - it can be inferred that the DBHE offers a slightly higher energy flow rate at the wellhead compared to the NWG 55-29 open-loop well with a percentage increase of 3.44%. It is important to note that this comparison is an estimate and in reality, $\dot{m}$ and c_P will vary considerably with depth.

A comparison between the two designs is also interpreted by assessing the bottomhole temperature at a fixed depth of $3067m$. Assuming no major temperature losses up the tubing ($\pm 5°C$), the temperature at the wellbore bottom can be regarded as the temperature at the outlet point.

The highest bottomhole temperature observed in this sensitivity analysis without significant heat loss up the tubing is $73.4°C$ for $3kg/s$ in the $\dot{m}$ parameter change, whereas the conventional open-loop NWG 55-29 wellbore reached a static bottomhole temperature of $331°C$ (Cladouhos et al, 2016). Both examples are at a fixed depth of $3067m$. Taking $\Delta q_{Th} = 0.956 - (-0.200) = 1.16MW$ as the simulated energy flow rate between the wellbore bottom and the inlet point for $3kg/s$, a comparison can be made with that obtained in the conventional NWG 55-29 well.

Assuming constant parameters $\dot{m} = 3kg/s$, $c_P = 4200J/kg°C$ for pure water and $\Delta T = 331 - 12 = 319°C$, then $q_{Th} = 4.02MW$ for the NWG 55-29 wellbore in comparison to $q_{Th} = 1.16MW$ for the DBHE design. This concludes that the closed-loop DBHE design offers an energy flow rate output approximately a factor of 3.5 lower than that of the conventional design.

However, the highest energy flow rate obtained in the $\dot{m}$ analysis was for $9kg/s$ - yielding $\Delta q_{Th} = 1.45 - (-0.614) = 2.06MW$ for a bottomhole temperature of $32.1°C$ in comparison to $q_{Th} = 12.1MW$ for the NWG 55-29 wellbore at a fixed $\dot{m} = 9kg/s$. This yields an energy flow rate drop for the DBHE of approximately a factor of 5.84 lower in comparison to the static NWG 55-29 bottomhole temperature of $331°C$.

These mass flow rates were chosen for comparison because according to (Cladouhos et al, 2016), similar values were obtained for an initial flow test ($9.5kg/s$ down to $5.7kg/s$ after 1 hour, with an average flow rate $3.2kg/s$).

The estimate of q_{Th} for NWG 55-29 carries some uncertainty, especially when defining c_P because phase changes will occur with depth and the specific heat capacity will change as a result of this. In the T2Well/EOS1 software, these phase changes are taken into account so the simulated energy flow rate values will carry accuracy. Nevertheless, it can be inferred that the closed-loop design is associated with a lower heat extraction potential compared to that of an operating EGS (assuming the EGS is successful) – especially when a lower $\dot{m}$ results in lower wellhead temperatures, according to (Alimonti et al, 2018).

However, a DBHE solution for the current NWG 55-29 well would not require stimulation to create an artificial reservoir, and hence less energy consumption is initially used up. Furthermore, the DBHE is a closed system, which enables easy monitoring and prevents fluid losses and pipe corrosion/blockage. For EGS projects where unexpected failures occur, the DBHE design could be an effective alternative. For example, an EGS site at Rosemanowes in Cornwall failed to create artificial fractures and suffered fluid loss of 70% - leading to project abandonment in 1991 (Lu, 2018). EGS activites in Cornwall, UK is ongoing and having the DBHE as a backup option could be beneficial, especially if drilling does not meet expectations.

While supercritical depths in the Newberry reservoir could not be modelled in this study due to software limitations, numerical wellbore-reservoir modelling will need to be further developed by adopting a supercritical equation of state (EOS1sc), see for example (Battistelli et al, 2020; Croucher and O'Sullivan, 2008), to assess the true thermal potential in these ultra-high temperature environments, notably targeted in the NDDP and IDDP projects.

It is also worth noting that only the thermal energy flow rate was quantified in this study. In fact, the overall net thermal capacity and total efficiency of the system should be investigated, considering the pumping power required for fluid circulation. Other future work entails:

- The return flow pressure at the bottom of the wellbore should be validated with another experimental study or Multiphysics software.
- Exploring a variety of working fluids, including water with salinity, carbon dioxide (Sun et al, 2019), or isobutane as a supercritical fluid (Wang et al, 2019).
- Investigating more complex unconventional DBHE designs, such as an artificial geyser concept (Heller et al, 2014).
- Investigating the effects of anisotropic reservoir permeability/porosity on DBHE thermal recovery.

Conclusion

An in-depth sensitivity analysis was performed with reference to a base-case DBHE design from (Morita et al, 1992b), and was modelled into the NWG 55-29 Newberry environment.

The best-case scenarios that offered maximal thermal efficiency was: $\dot{m} = 5kg/s$, an insulated inner tubing for Casg1 of $\lambda = 0.01038W/mK$, maintaining a high

λ for the outer casings (Casg2, Casg3) and the cement layers (Ceme1, Ceme2) and increasing the annulus radii (Case2), with a resulting thermal output $q_{Th} = 1.50MW$.

Each parameter change offered some interesting insights. Altering the mass flow rate influenced the working fluid's velocity and its residence time down the annulus. An insulated inner tubing limits heat losses and minimises ΔT up the tubing. The outer casing properties do not significantly affect the heat transfer inside the wellbore, but should not be insulated to ensure sufficient heat transfer occurs between the reservoir and wellbore. The cement properties lead to a higher q_{Th} when λ was maximised and the use of graphite flakes in a conductive filler as opposed to conventional cement appears to be an efficient, though unproved concept, yielding a percentage increase in energy flow rate of 14.4% ($q_{Th} = 2.32MW$). Adjusting the radii dimensions will affect the residence time of the working fluid, similar to the sensitivity analysis conducted for varying the mass flow rate.

An energy flow rate comparison was made between this study and the conventional NWG 55-29 EGS well. The results showed that the DBHE was a factor of 3.5 and 5.84 lower when assuming constant mass flow rates of $3kg/s$ and $9kg/s$, respectively. While the DBHE design has a lower heat extraction and efficiency compared to conventional EGS designs, when the latter are feasible, it can mitigate typical EGS risks e.g. induced seismicity, fluid losses and contamination. Future EGS projects should therefore consider the DBHE as an alternative design in situations where drilling may achieve original projects expectations.

Further work is needed to fully quantify the potential of the DBHE concept. The use of Multiphysics software and/or experimental data will be useful to validate the uncertainties in the pressure losses from the return fluid at the wellbore bottom. In addition, a variety of working fluid's and unconventional DBHE designs should be explored. Numerical wellbore-reservoir modelling tools will need to be further developed for supercritical environments, using the IDDP and NDDP projects for initial verification and calibration.

Abbreviations

List of symbols

κ: index for the working fluid; V: volume (m^3); n: outward normal vector; Γ: surface area of well side (m^2); M^κ: mass accumulation term; F^κ: key mass/energy transport terms; q^κ: key source/sink terms; ϕ: porosity; S: local saturation of phase; ρ: density of phase (kg/m^3); X mass fraction of water in phase; u: velocity of fluid (m/s); c specific heat capacity $(J/kg^\circ C)$; T: temperature $(^\circ C)$; U: specific thermal energy in the phase; λ: thermal conductivity (W/mK); h: specific enthalpy in phase; (kJ/kg); k: permeability $(m^2 or Darcy)$; μ_{ph}: phase viscocity of the fluid $(Paseconds)$; P: pressure (Pa); g: gravitational acceleration (m/s^2); z: elevation in well (m); θ: inclination angle of wellbore $(^\circ)$; A: cross sectional area of wellbore (m^2); C_0: profile parameter; j: volumetric flux of mixture (m/s); K: function to smooth transition of drift velocity from fluid stages; K_u: Kutateladze number; $m(\theta)$: inclination of wellbore; γ: slip between two phases; f: apparent friction coefficient; $\dot{m}$: mass flow rate (kg/s); r: horizontal radii dimension (m); ΔT: change in temperature up tubing or down annulus $(^\circ C)$; q_{Th}: energy flow rate (MW).

Subscripts

ph: phase; L: liquid phase; G: gaseous phase; R: rock properties; a: absolute permeability; r, ph: relative permeability of a certain phase d: drift velocity; c: characteristic velocity; m mixture;i: inlet; o: outlet; F: working fluid at wellbore bottom.

Acronyms

DBHE: deep borehole heat-exchanger; EGS: Enhanced Geothermal System; SEGS: Supercritical Enhanced Geothermal System; NDDP: Newberry Deep Drilling Project; IDDP: Icelandic Deep Drilling Project; HDR: hot deep rock; SHR: super hot rock.

Acknowledgements

I would like to Acknowledge Dr Xiaolei Liu for initial assistance in T2Well/EOS1 software manipulation.

Author's contributions
TR assisted in numerical validation section and general advice on journal layout. LP and TR assisted in T2Well/EOS1 software manipulation. All Authors have read and approved the final manuscript.

Funding
This research is supported by the UK Engineering and Physical Sciences Research Council (EPSRC) [Grant number EP/RS13222/1]

Availability of data and materials
The datasets used and/or analysed during the current study are available from the corresponding author on reasonable request.

Competing interests
The authors declare that they have no competing interests.

Author details
[1]James Watt, School of Engineering, University of Glasgow, G12 8QQ Glasgow, UK. [2]Energy and Power, Cranfield University, MK43 0AL Cranfield, UK. [3]Earth Sciences Division 90-1116, Lawrence Berkeley National Laboratory, 95720, CA USA.

References
Acuña J, Mogensen P, Palm B (2011) Distributed thermal response tests on a multi-pipe coaxial borehole heat exchanger. HVAC and R Research 17(6):1012–1029,
Akbar S, Fathianpour N, Al Khoury R (2016) A finite element model for high enthalpy two-phase flow in geothermal wellbores. Renewable Energy 94:223–236,
Alimonti C, Soldo E (2016) Study of geothermal power generation from a very deep oil well with a wellbore heat exchanger. Renewable Energy 86:292 – 301, , URL http://www.sciencedirect.com/science/article/pii/S0960148115302317
Alimonti C, Berardi D, Bocchetti D, Soldo E (2016) Coupling of energy conversion systems and wellbore heat exchanger in a depleted oil well. Geothermal Energy 4(1):11, , URL https://doi.org/10.1186/s40517-016-0053-9
Alimonti C, Soldo E, Bocchetti D, Berardi D (2018) The wellbore heat exchangers: A technical review. Renewable Energy 123:353–381,
Asadi I, Shafigh P, Abu Hassan ZFB, Mahyuddin NB (2018) Thermal conductivity of concrete – a review. Journal of Building Engineering 20:81–93,
Asl AH, Khajenoori M (2013) Subcritical water extraction. In: Nakajima H (ed) Mass Transfer, IntechOpen, Rijeka, chap 17, , URL https://doi.org/10.5772/54993
Battistelli A, Finsterle S, Marcolini M, Pan L (2020) Modeling of coupled wellbore-reservoir flow in steam-like supercritical geothermal systems. Geothermics 86:101,793, , URL http://www.sciencedirect.com/science/article/pii/S0375650519302652
Beier RA, Acuña J, Mogensen P, Palm B (2013) Borehole resistance and vertical temperature profiles in coaxial borehole heat exchangers. Applied Energy 102:665 – 675, , URL http://www.sciencedirect.com/science/article/pii/S0306261912005764, special Issue on Advances in sustainable biofuel production and use - XIX International Symposium on Alcohol Fuels - ISAF
Bertani R, Büsing H, Buske S, Dini A, Hjelstuen M, Luchini M, Manzella A, Nybo R, Rabbel W, Serniotti L, Science D, Team T (2018) The first results of the descramble project. SGP-TR : Stanford Geothermal Program workshop report, vol 213
Bonneville A, Cladouhos TT, Petty S, Schultz A, Sørlie C, Asanuma H, FriÃleifsson GO, Jaupart C, de Natale G (2018) The newberry deep drilling project (nddp) workshop. Scientific Drilling 24:79–86, , URL https://www.sci-dril.net/24/79/2018/
Breede K, Dzebisashvili K, Liu X, Falcone G (2013) A systematic review of enhanced (or engineered) geothermal systems: past, present and future. Geothermal Energy 1(1), , URL http://eprints.gla.ac.uk/169706/
Cladouhos TT (2012) Newberry well 55-29 stimulation data: casing-cement-thermal-properties.xlsx. URL https://openei.org/doe-opendata/dataset/newberry-well-55-29-stimulation-data
Cladouhos TT, Petty S, Swyer MW, Uddenberg ME, Grasso K, Nordin Y (2016) Results from newberry volcano egs demonstration, 2010–2014. Geothermics 63:44–61,
Cladouhos TT, Petty S, Bonneville A, Schultz A, Sorlie CF (2018) Super hot egs and the newberry deep drilling project. In: 43rd Workshop on Geothermal Reservoir Engineering, pp 1–13
Croucher AE, O'Sullivan MJ (2008) Application of the computer code tough2 to the simulation of supercritical conditions in geothermal systems. Geothermics 37(6):622–634,
DEEPEGS (2018) Iddp-2 way forward workshop, saga report no.11. Report
DEEPEGS (2019) Iddp-2 flow test kick-off meeting, saga report no.12. Report
DiPippo R (2015) Geothermal Power Plants Principles, Applications, Case Studies and Environmental Impact. Chapter 1: Geology of geothermal regions, Elsevier Ltd, USA, pp 1–20.
Dobson P, Asanuma H, Huenges E, Poletto F, Reinsch T, Sanjuan B (2017) Supercritical geothermal systems - a review of past studies and ongoing research activities. In: 41st Workshop on Geothermal Reservoir Engineering, pp 1–13
Doran H (2019) Modelling closed-loop supercritical geothermal wells, master thesis. Master's thesis
Falcone G, Liu X, Okech RR, Seyidov F, Teodoriu C (2018) Assessment of deep geothermal energy exploitation methods: The need for novel single-well solutions. Energy 160:54–63,
Heller C, Teodoriu C, Falcone G (2014) Harnessing deep geothermal heat using a new concept based on the geyser principle. In: Thirty-Ninth Workshop on Geothermal Reservoir Engineering, pp 1–8

Higgins B, Oldenburg C, Muir M, Pan L, Eastman A (2016) Process modelling of a closed-loop sco2 geothermal power cycle. In: 5th International Supercritical CO2 Power Cycles Symposium in Texas 2016, pp 1–12

Holmberg H, Acuña J, Næss E, Sønju OK (2016) Thermal evaluation of coaxial deep borehole heat exchangers. Renewable Energy 97:65 – 76, , URL http://www.sciencedirect.com/science/article/pii/S096014811630458X

Hu X, Banks J, Wu L, Liu WV (2020) Numerical modeling of a coaxial borehole heat exchanger to exploit geothermal energy from abandoned petroleum wells in hinton, alberta. Renewable Energy 148:1110 – 1123, , URL http://www.sciencedirect.com/science/article/pii/S0960148119314855

Ichim A, Teodoriu C, Falcone G (2016) Influence of cement thermal properties on wellbore heat exchange. In: 41st Workshop on Geothermal Reservoir Engineering, p 8

IEA (2011) Technology roadmap - geothermal heat and power. Tech. rep., France

IFC (1967) The 1967 IFC formulation for industrial use : a formulation of the thermodynamic properties of ordinary water substance. Dusseldorf : IFC Secretariat

Kim KH, Ree JH, Kim Y, Kim S, Kang SY, Seo W (2018) Assessing whether the 2017 mw 5.4 pohang earthquake in south korea was an induced event. Science 360(6392):1007–1009, , URL https://science.sciencemag.org/content/360/6392/1007, https://science.sciencemag.org/content/360/6392/1007.full.pdf

Kohl T, Salton M, Rybach L (2000) Data analysis of the deep borehole heat exchanger plant weissbad (switzerland). In: Proceedings World Geothermal Congress 2000, pp 3459–3464

Kohl T, Brenni R, Eugster W (2002) System performance of a deep borehole heat exchanger. Geothermics 31:687–708

Lu SM (2018) A global review of enhanced geothermal system (egs). Renewable and Sustainable Energy Reviews 81:2902–2921,

MIT (2006) The future of geothermal energy, impact of enhanced geothermal systems (egs) on the united states in the 21st century. Tech. Rep. INL/EXT-06-11746, MIT, Massachusetts

Morita K, Matsubayashi O, Kusunoki Ki (1985) Down-hole coaxial heat exchanger using insulated inner pipe for maximum heat extraction. Geothermal Resources Council Transactions 9(1):45–50

Morita K, Bollmeier WS, Mizogami H (1992a) Analysis of the results from the downhole coaxial heat exchanger (dche) experiment in hawaii

Morita K, Bollmeier WS, Mizogami H (1992b) An experiment to prove the concept of the downhole coaxial heat exchanger (dche) in hawaii

Muraoka H, Asanuma H, Tsuchiya N, Ito T, Mogi T, Ito H, the participants of the ICDP/JBBPWorkshop (2014) The japan beyond-brittle project. Scientific Drilling 17:51–59, , URL https://www.sci-dril.net/17/51/2014/

Nalla G, Shook GM, Mines GL, Bloomfield KK (2005) Parametric sensitivity study of operating and design variables in wellbore heat exchangers. Geothermics 34(3):330–346,

Nuclear-powernet (2019) What is nusselt number. URL https://www.nuclear-power.net/nuclear-engineering/heat-transfer/introduction-to-heat-transfer/characteristic-numbers/what-is-nusselt-number/

Olasolo P, Juárez MC, Morales MP, D'Amico S, Liarte IA (2016) Enhanced geothermal systems (egs): A review. Renewable and Sustainable Energy Reviews 56:133–144,

Pan L, Oldenburg CM (2014) T2well—an integrated wellbore–reservoir simulator. Computers & Geosciences 65:46 – 55, , URL http://www.sciencedirect.com/science/article/pii/S0098300413001696, tOUGH Symposium 2012

Pan L, Spycher N, Doughty C, Pruess K (2005) Eco2n v2.0: A new tough2 fluid property module for mixtures of water, nacl and co2

Pan L, Oldenburg C, Wu YS, Pruess K (2011) T2well/eco2n version 1.0:

Pan L, Oldenburg CM, Freifeld BM, Jordan PD (2018) Modeling the aliso canyon underground gas storage well blowout and kill operations using the coupled well-reservoir simulator t2well. Journal of Petroleum Science and Engineering 161:158 – 174, , URL http://www.sciencedirect.com/science/article/pii/S0920410517309488

Pruess K, Oldenburg C, Moridis G (2012) Tough2 user's guide, version 2

Raymond J, Mercier S, Nguyen L (2015) Designing coaxial ground heat exchangers with a thermally enhanced outer pipe. Geothermal Energy 3(1):7, , URL https://doi.org/10.1186/s40517-015-0027-3

Reinsch T, Dobson P, Asanuma H, Huenges E, Poletto F, Sanjuan B (2017) Utilizing supercritical geothermal systems: a review of past ventures and ongoing research activities. Geothermal Energy 5(1):1–25,

Renaud T, Stebel M, Verdin P, Falcone G (2018) Cfd modeling of a high enthalpy geothermal context. In: 43rd Workshop of Geothermal Reservoir Engineering, pp 1–8

Renaud T, Verdin P, Falcone G (2019) Numerical simulation of a deep borehole heat exchanger in the krafla geothermal system. International Journal of Heat and Mass Transfer 143:118,496, , URL http://www.sciencedirect.com/science/article/pii/S0017931019312049

Renaud T, Pan L, Doran H, Falcone G, Verdin PG (2020) Numerical analysis of enhanced conductive deep borehole heat exchangers. Geothermics pending publication:1–10

Sammel EA, Ingebritsen SE, Mariner RH (1988) The hydrothermal system at newberry volcano, oregon. Journal of Geophysical Research: Solid Earth 93(B9):10,149–10,162,

Seyidov F (2016) Investigation of the feasibility and efficiency of deep borehole heat exchangers, master thesis. Master's thesis

Song X, Zheng R, Li G, Shi Y, Wang G, Li J (2018) Heat extraction performance of a downhole coaxial heat exchanger geothermal system by considering fluid flow in the reservoir. Geothermics 76:190–200,

Sonnenthal E, Spycher N, Callahan O, Cladouhos TT, Petty S (2012) A thermal-hydrological-chemical model for the enhanced geothermal system demonstration project at newberry

Sudarmadi E, Zarrouk SJ, Croucher AE, Bramantyo EA (2012) Modelling production from supercritical geothermal reservoirs. In: New Zealand Geothermal Workshop 2012 Proceedings, vol 40, pp 1–6

Sui D, Wiktorski E, Røksland M, Basmoen TA (2019) Review and investigations on geothermal energy extraction from abandoned petroleum wells. Journal of Petroleum Exploration and Production Technology 9(2):1135–1147, , URL https://doi.org/10.1007/s13202-018-0535-3

Sun X, Wang Z, Liao Y, Sun B, Gao Y (2019) Geothermal energy production utilizing a u-shaped well in combination with supercritical co2 circulation. Applied Thermal Engineering 151:523–535,

Tang H, Xu B, Hasan AR, Sun Z, Killough J (2019) Modeling wellbore heat exchangers: Fully numerical to fully analytical solutions. Renewable Energy 133:1124–1135,

Toth A (2015) Flow and Heat Transfer in Geothermal Systems. Chapter 13: Borehole Heat Exchangers, Elsevier Inc, pp 287–298.

Wang Y, Zhang L, Cui G, Kang J, Ren S (2019) Geothermal development and power generation by circulating water and isobutane via a closed-loop horizontal well from hot dry rocks. Renewable Energy 136:909–922,